JCTC Journal of Chemical Theory and Computation

pubs.acs.org/JCTC Article

Genetic Algorithm Driven Force Field Parameterization for Molten Alkali-Metal Carbonate and Hydroxide Salts

Anirban Mondal, Jeffrey M. Young, Timothy A. Barckholtz, Gabor Kiss, Lucas Koziol,* and Athanassios Z. Panagiotopoulos*

Cite This: *J. Chem. Theory Comput.* 2020, 16, 5736−5746 Read Online

ACCESS | Metrics & More | Article Recommendations | Supporting Information

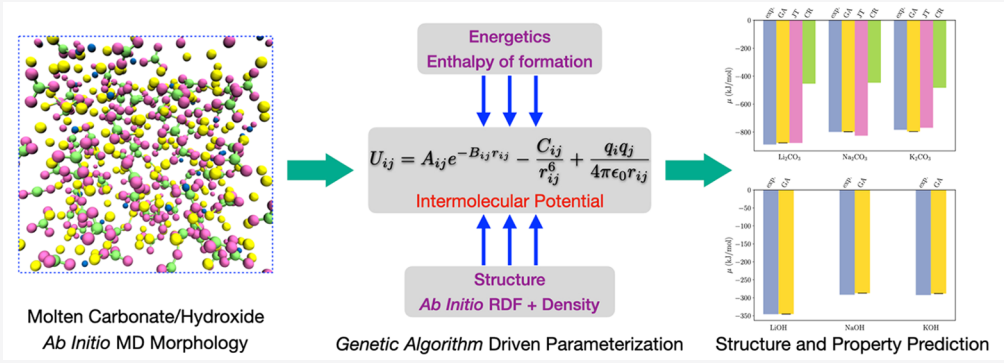

ABSTRACT: Molten alkali-metal carbonates and hydroxides play important roles in the molten carbonate fuel cell and in Earth's geochemistry. Molecular simulations allow us to study these systems at extreme conditions without the need for difficult experimentation. Using a genetic algorithm to fit *ab intio* molecular dynamics-computed densities and radial distribution functions, as well as experimental enthalpies of formation, we derive new classical force fields able to accurately predict liquid chemical potentials. These fitting properties were chosen to ensure accurate liquid phase structure and energetics. Although the predicted dynamics is slow when compared to experiments, in general the trends in dynamic properties across different systems still hold true. In addition, these newly parametrized force fields can be extended to the molten carbonate−hydroxide mixtures by using standard combining rules.

1. INTRODUCTION

Molten alkali-metal carbonates and hydroxides have melting points significantly above room temperature, often by several hundred degrees. They have many attractive properties such as high ionic and thermal conductivity, chemical stability, and low vapor pressure.[1,2] As a result, they are actively studied for electrolytes in electrochemical batteries and fuel cells.[3,4] Molten carbonate salts in the Earth's mantle are present as highly conductive phases that are known to play important geophysical roles, including as a long-term deep storage medium for carbon.[1,5]

In this article, we focus on obtaining force fields with accurate chemical potentials for the carbonate and hydroxide salts of the alkali-metals Li, Na, and K to develop a better understanding of the electrolytes employed in molten carbonate fuel cells (MCFCs). MCFCs are commercially used for power generation, but they are also a promising technology for recovering carbon dioxide (CO_2) from flue gases, for example, in natural-gas or coal-fired power plants, refineries, chemical plants, etc.[6−8]

MCFCs use the electrochemical driving force of hydrogen (H_2) reacting with oxygen (O_2) to concentrate CO_2 on the anode side while simultaneously generating electricity. The electricity generated offsets the cost of CO_2 capture, potentially making this process more economical than traditional carbon capture methods that use liquid amine absorbers.[9,10] Most MCFC electrolytes are binary eutectic carbonates, $M_1M_2CO_3$, with M_1 and M_2 typically being Li^+/K^+ or Li^+/Na^+.

During MCFC operation, CO_2 and O_2 form carbonate ions, CO_3^{2-}, in the electrolyte on the cathode side. The carbonate ions travel via ionic conduction across the fuel cell to the anode, where they react in the presence of H_2 to form water, releasing CO_2. The resulting anode gas effluent contains highly concentrated CO_2 (∼70% dry basis)[11] which can be further purified and reused or sequestered. In addition to CO_2 and O_2, water vapor is also typically present in MCFC cathode feeds. It

Received: March 24, 2020
Published: July 24, 2020

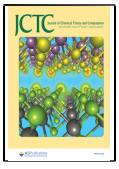

https://dx.doi.org/10.1021/acs.jctc.0c00285
J. Chem. Theory Comput. 2020, 16, 5736−5746

can react with CO_3^{2-} in the electrolyte to exchange carbonate and hydroxide ions, via the carbonate hydrolysis equilibrium in eq 1.

$$CO_3^{2-}(l) + H_2O(g) \leftrightarrow 2OH^-(l) + CO_2(g) \quad (1)$$

The equilibrium shifts to the right as CO_2 is removed from the cathode gas, especially when the MCFC is driven to maximize CO_2 removal from the cathode gas for carbon capture. Therefore, in carbon capture operations, the electrolyte may actually be a mixed carbonate/hydroxide rather than a pure carbonate phase. In a recent experiment, Rosen et al. demonstrated that hydroxide can be a parallel charge carrier when water is present in the cathode gas and CO_2 concentrations are driven to a low level, e.g., <1 mol %.[12] Because it transports charge but not CO_2, this parallel hydroxide route reduces the overall carbon capture efficiency. Clearly, a better understanding of hydroxide formation in carbonate melts and its effects on properties, especially ionic conductivity and volatility, would be useful in the design of new electrolytes that minimize noncarbonate charge transport. Unfortunately, experimental characterization of the electrolyte is challenging due to high operating temperatures (above 600 °C). Therefore, molecular simulations, particularly both *ab initio* (AIMD) and classical molecular dynamics (MD), can play a role in advancing our understanding of the challenging problem of MCFC electrolytes reacting with a multicomponent gas phase.

In order to investigate the reaction equilibrium of eq 1 using molecular simulations (reported in a separate paper[13]), the concentration dependence of the chemical potential of carbonate and hydroxide ions is required. Chemical potential calculations require longer simulations than are currently feasible with *ab initio* techniques. Classical MD can reach these nanosecond time scales, but it needs force fields with accurate energetics. Only a few force fields (FFs) have been reported in the literature describing alkali-metal carbonates[14−17] and hydroxides[18] and none to our knowledge describing mixed carbonate/hydroxides. The most well-known FF for carbonates was developed by Janssen and Tissen (JT)[14] for the unary Li_2CO_3, Na_2CO_3, and K_2CO_3 salts. They used a rigid model for the carbonate ion, point charges (+1e on the cations and −2e on the carbonate ions) for the Coulomb interaction, and exponential repulsion for the ion cores. Model parameters were fitted using *ab initio* interaction energies. Recently, significant improvement toward an accurate description of the physical properties of molten carbonates and their eutectic mixtures came with the force fields of Corradini et al. (CR).[16,17] They used the Buckingham interaction potential (exponential repulsion and $1/r^6$ attraction) with scaled Coulomb interactions (total charges on each ion scaled by 0.821). The van der Waals (vdW) parameters were manually optimized to better reproduce not only densities but also AIMD-computed radial distribution functions (RDFs). Importantly, the FF was transferable to several properties not included in the fitting data set, namely, self-diffusion constants, ionic conductivities, and viscosities.

Since our goal is to investigate reaction equilibria, we need to evaluate the existing force fields by their ability to predict liquid phase chemical potential and density of unary carbonate salts. While the JT model performs well in predicting chemical potentials with a maximum deviation of ∼25 kJ/mol for Na_2CO_3, it predicts a density 10−20% below experimental values. On the other hand, the CR model is able to reproduce good densities but gives a considerably more positive chemical potential than experiments. Details of these comparisons are provided in Section 3.3 below. Since neither of these force fields can simultaneously give both accurate chemical potential and density, we need a new set of force field parameters for the carbonate salts.

One classical force field has been reported for molten hydroxides. This model by Okazaki et al.[18] assumes a rigid O−H bond, and the interaction potential between atoms is given by a sum of Buckingham type nonbonded term and $1/r^4$ interaction. Such a nontrivial potential function requires additional modification within the simulation program to account for the long-range interactions and is not compatible with the existing carbonate potentials' forms. Thus, there is a strong need to obtain a force field for hydroxides that can be used in combination with carbonate force fields in mixtures relevant for MCFCs. This is one of the main objectives of the current work.

In this work, we develop a consistent set of force fields to treat both carbonates and hydroxides using the same functional form and fitting procedure. We use these force fields to compute several thermodynamic, structural, and transport properties. This paper is organized as follows. Section 2 describes the computational details of AIMD simulations, force field development, and classical MD simulations. Section 3 presents the parametrized force field and the results of our MD simulations for the fitted properties set. We also compare the accuracy of AIMD to the experimental densities of molten carbonates and hydroxides. We then use the new force fields to compute several properties not part of the fitting set, including chemical potentials. Finally, Section 4 presents our conclusions.

2. METHODS

2.1. *Ab Initio* MD. All AIMD calculations were performed using the PBE exchange-correlation functional[19] with Grimme's D3 treatment of dispersion[20] as implemented in the CP2K program.[21] A planewave cutoff of 800 Ry was used throughout, with four multigrids to represent the density. Atomic orbitals were represented by double-ζ polarizable (DZP) basis functions of GTH.[22,23] Simulations of the liquids in the isothermal−isobaric (*NPT*) ensemble were performed at 1 bar using an isotropic unit cell according to the scheme of Martyna et al.,[24] with a time constant of 500 fs. Both *NPT* and canonical (*NVT*) simulations utilized one chain of six Nosé−Hoover thermostats[25] and a 100 fs time constant. The simulation temperatures were set to 1043.15, 1173.15, and 1213.15 K for Li_2CO_3, Na_2CO_3, and K_2CO_3, respectively, whereas simulations were performed at 923.15 K for all studied hydroxides. All AIMD calculations utilized a 1 fs MD time step.

Fully periodic unit cells containing 150 cations were used throughout. The number of anions varied from 75 for pure carbonates to 150 for pure hydroxides. For all AIMD compositions, the total number of atoms was 450. Recently, Bengston et al.[26] showed that for Li, K, and Li/K eutectic chlorides (broadly similar to carbonates), AIMD unit cells containing approximately 216 atoms, with simulation times of 6−12 ps, were sufficient to converge properties including density, thermal expansion, bulk modulus, and self-diffusion constants. All compositions were equilibrated in the *NPT* ensemble for 50 ps which was followed by production runs of 25 ps in the *NVT* ensemble to calculate the RDFs. Molten salt

https://dx.doi.org/10.1021/acs.jctc.0c00285
J. Chem. Theory Comput. 2020, 16, 5736−5746

densities were computed from the average cell volumes over the last 25 ps of the 50 ps *NPT* trajectory.

2.2. Force Field: Functional Form. For the proposed classical force fields, the interaction energy between atom i and j is computed as a sum of the Buckingham and Coulomb interaction terms:

$$U_{ij} = A_{ij}e^{-B_{ij}r_{ij}} - \frac{C_{ij}}{r_{ij}^6} + \frac{q_i q_j}{4\pi\epsilon_0 r_{ij}} \quad (2)$$

where A_{ij} and B_{ij} describe the repulsive part of the interaction, C_{ij} is the dispersive part of the Buckingham interaction, r_{ij} is the distance between the two atoms, and q is the charge on each atom. The adjustable parameters consist of atom-centered point charges $\{q_i\}$ (summing to +1e on cations, −1e on the hydroxide ion, and −2e on the carbonate ion) and Buckingham parameters $\{A_{ij}, B_{ij}, C_{ij}\}$. Similar to the CR model,[16] we first reduced the number of parameters by limiting Buckingham interactions to a subset of atom type pairs. Specifically, Buckingham interactions were defined only for $M-O_{CO_3}$ and $O_{CO_3}-O_{CO_3}$ in carbonates (where M is one of Li, Na, K) and $M-O_{OH}$, $O_{OH}-O_{OH}$, and $O_{OH}-H$ in hydroxides. All other interactions are purely Coulombic. This led to 13 independent parameters to be optimized for carbonates and 16 for hydroxides. We then fitted the three M_2CO_3 and three MOH salts separately to AIMD densities, AIMD M−O and O−O RDFs, and the experimental enthalpy of formation of the liquid from separated gas-phase ions, $\Delta_f H$, as defined in Section 1 of the Supporting Information. Fitting to density and RDFs ensures accurate structure whereas $\Delta_f H$ constrains the intermolecular interactions to obtain accurate energetics.

2.3. Force Field: Parameter Optimization. The numerical optimization of multiple independent variables is challenging due to the strong couplings between different atom types and between Coulomb versus dispersion interactions. These factors must be balanced so that molecules remain in a narrow range of intermolecular distances. The number of physically realistic solutions is small relative to the parameter space, in the sense that randomly generated parameters overwhelmingly lead to nonphysical FFs, with unit cells either collapsing or exploding within ∼100 fs. Local optimization starting from random parameters was also inefficient since the starting points are often far from local minima with qualitatively good performance. Therefore, we decided to use a genetic algorithm (GA) approach for parameter optimization. GAs were recently shown to be an efficient stochastic global optimization method for parametrizing force fields with a large number of parameters (e.g., more than 10).[27]

Before starting the GA, we found it crucial to perform a prescreening of the parameters to identify individuals with higher quality than randomly generated parameters. We first tried to perform local optimizations on the initial randomized parameter sets, but in all test cases the nearest local minima did not have qualitatively better performance than the initial guess. We found it much more efficient to screen the randomized vectors by single-point energies as shown in Figure 1. Starting from random-valued trial parameters, we performed three test calculations of increasing cost to remove unphysical parameters as efficiently as possible. All the tests were started from liquid configurations that were taken from AIMD trajectories and then optimized to the nearest local minimum using density functional theory (DFT).

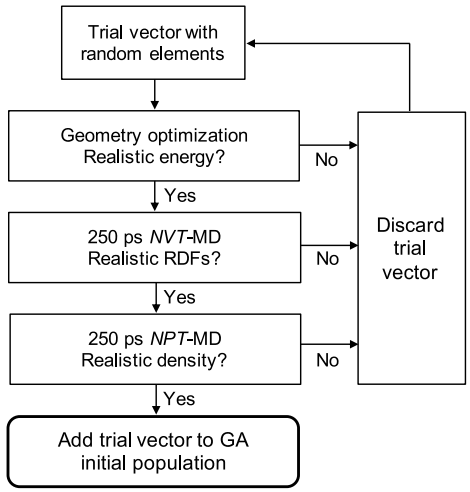

Figure 1. Schematic of the prescreening procedure for computing an initial genetic algorithm (GA) population of force field vectors.

In the first test, the liquid configuration from AIMD was optimized using the trial FF parameters, and the average energy per unit species (either unary carbonate, M_2CO_3, or unary hydroxide, MOH) calculated by the trial FF was compared to DFT. If the difference was within ±100 kJ/mol, the parameters were retained. In the second test, a short *NVT* MD simulation was performed (at the same density as AIMD), and the M−M, M−O, and O−O RDFs were compared to AIMD RDFs. If the average root-mean-square deviation (RMSD) was below an arbitrary cutoff value, the parameters were retained. We chose a cutoff of 0.1, based on visual comparison of several FF RDFs to AIMD RDFs. In the third test, the liquid density was computed from an *NPT* MD simulation. If the density was within ±50 kg/m^3 of AIMD, the trial parameters were retained. Otherwise, they were discarded, and the process was restarted with new trial parameters. Using this workflow, we were able to screen through ∼10^7 guess vectors to generate several thousand individuals that could be used for the GA. Prescreening has very low computational cost because it does not couple trial vectors and also can discard a trial vector without evaluating the entire objective function.

Our approach for GA optimization is shown in Figure 2. We started from an initial population of N trial parameters, generated using the procedure in Figure 1. We then applied a series of genetic operators to create a temporary population, set to $10N$. Offspring individuals were then created by randomly selecting each parameter from one of two parent individuals. In addition, mutations were introduced by changing the value of a parameter by ±5% with a 10% probability.

The fitness of offsprings was calculated according to a fitness function, F, containing density, RDFs, and enthalpy components:

$$F_{\text{density}} = |D_{\text{FF}} - D_{\text{AIMD}}| \quad (3)$$

$$F_{\text{RDF}} = \frac{1}{3}(\text{RMSD}_{\text{FF,AIMD}}(\text{RDF}^{\text{M-M}}) + \text{RMSD}_{\text{FF,AIMD}}(\text{RDF}^{\text{M-O}}) + \text{RMSD}_{\text{FF,AIMD}}(\text{RDF}^{\text{O-O}})) \quad (4)$$

$$F_{\Delta_f H} = |\Delta_f H_{\text{FF}} - \Delta_f H_{\text{Exp}}| \quad (5)$$

https://dx.doi.org/10.1021/acs.jctc.0c00285
J. Chem. Theory Comput. 2020, 16, 5736−5746

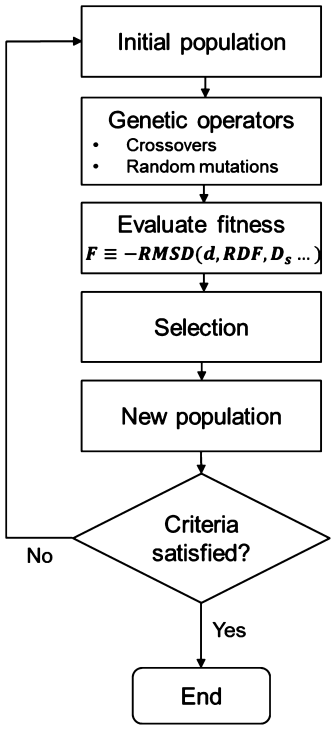

Figure 2. Schematic of the genetic algorithm workflow to optimize M_2CO_3 or MOH parameter sets.

where D, RMSD, and $\Delta_f H$ correspond to densities, RMSD between RDFs, and enthalpy of formation, respectively, computed via 250 ps *NPT* and 250 ps *NVT* molecular dynamics simulations with 75 M_2CO_3 or 150 MOH molecules (same as in AIMD) according to the details in Section 2.5 below. The total fitness function is a weighted sum of the three components

$$-F = w_{\text{density}} F_{\text{density}} + w_{\text{RDF}} F_{\text{RDF}} + w_{\Delta_f H} F_{\Delta_f H} \quad (6)$$

where the weights are necessary to account for different units. F_{density} has units of kg/m^3, and w_{density} equals 10^{-3} (kg/m^3)$^{-1}$. F_{RDF} is unitless because RDFs are unitless, and $w_{\text{RDF}} = 1$. $F_{\Delta_f H}$ has units of kJ/mol, and $w_{\Delta_f H}$ equals 10^{-4} (kJ/mol)$^{-1}$. Root-mean square deviations (RMSDs) of the radial distribution functions were calculated according to the following equation:

$$\text{RMSD}_{\text{FF,AIMD}} = \sqrt{\frac{\sum_d (\text{RDF}_{\text{FF}}(d) - \text{RDF}_{\text{AIMD}}(d))^2}{N_d}} \quad (7)$$

where d is a set of distances over which the RDFs were evaluated, in the range of from 2.5 to 8.0 Å, with spacing 0.025 Å. In this expression, the superscripts labeling the RDF (M−O or O−O) are omitted for clarity. The exact values of the weights were unimportant as long as each term in eq 6 is of similar magnitude; we found the GAs to evolve to very similar parameters across a fairly broad range.

The population size for the GA was set to N = 500, with temporary offspring populations of 5000, which was limited for practical reasons of computational cost. Evolving one generation of the GA thus required a 2.5 μs MD simulation time. GAs were evolved for ∼10 generations, depending on convergence behavior, at which point the fitness distribution of the population became narrow and differences between individual fitnesses were approximately within the error bars of computed densities and RDFs due to the finite MD trajectories. The most fit individuals after 10 generations reproduced the AIMD densities to within about 1% and $\Delta_f H$ to within 10−20 kJ/mol. Since individual parameters have not seen any local optimization, as a last step we performed local optimization to converge $\Delta_f H$ to <1 kJ/mol of the reference values.

2.4. Intramolecular Potential. The oxygen−carbon−oxygen angles and the improper dihedral in a CO_3^{2-} ion were parametrized from first-principles scans (density functional theory, DFT-based) of the corresponding degrees of freedom and then matching first-principles and force field potential energy surfaces. All these calculations were performed at the B3LYP/6-311g+(d,p) level of theory using the Gaussian16 program.[28] For a given degree of freedom ϕ, constrained geometry optimizations were carried out on an isolated ion using both DFT and the force field levels, yielding the total energies $U_{\text{DFT}}(\phi)$ and $U_{\text{FF}}(\phi)$, respectively. The missing force field terms are then fitted to this difference using a quadratic potential form, $U(\phi) = \frac{1}{2}k_{\text{eq}}(\phi - \phi_{\text{eq}})^2$. Fits for the O−C−O angle and O−C−O−O improper dihedral are shown in Figures S1 and S2 of the Supporting Information. The hydroxide O−H bond was treated as rigid.

2.5. Classical Molecular Dynamics. We employed the GROMACS simulation program, v.2018,[29,30] to perform classical molecular dynamics simulations. The equations of motion were integrated with a time step of 1 fs. The leapfrog (MD) algorithm was used to integrate the equations of motion in all simulations except when computing $\mu^{\text{EX}}_{\text{vdW}}$ (as defined later in the Chemical Potential section) and the enthalpy of isolated molecules. For these simulations, we employed an efficient leapfrog stochastic dynamics (SD) integrator to integrate the equations of motion. The SD integrator ensures a better sampling of the states at which the inserted ion is weakly interacting with the rest of the system or when a single ion is present in the simulation cell. The long-range electrostatic interactions were treated using a smooth particle mesh Ewald technique with a real-space cutoff of 1.0 nm. For the Buckingham interactions, long-range corrections to energy and pressure were applied. The velocity-rescale thermostat[31] was employed to maintain the temperature in simulations that used the MD integrator, but all dynamical properties were calculated from *NVE* simulations without a thermostat. For all constant pressure simulations, the system pressure was controlled by using the Parrinello−Rahman barostat.[32] The O−H covalent bond was constrained via the LINCS constraint algorithm. All the physical properties were computed using a system composed of 1000 cations and 500 carbonate or 1000 hydroxide anions.

2.6. Chemical Potential. The chemical potential (μ) of the unary molten carbonate and hydroxide salts was calculated by splitting μ as in eqs 8 and 9.

$$\mu_{M_2CO_3} = 2\Delta_f G^0_{M^+} + \Delta_f G^0_{CO_3^{2-}} + \mu^{\text{IG}}_{M_2CO_3} + \mu^{\text{EX}}_{M_2CO_3} \quad (8)$$

$$\mu_{\text{MOH}} = \Delta_f G^0_{M^+} + \Delta_f G^0_{OH^-} + \mu^{\text{IG}}_{\text{MOH}} + \mu^{\text{EX}}_{\text{MOH}} \quad (9)$$

Here $\Delta_f G^0$ represents the Gibbs free energy of formation for each species from the standard state of each constituent atom, μ^{IG} is the ideal gas part of the chemical potential, and μ^{EX} is the excess part of the chemical potential. The free energy of formation is tabulated for neutral species and monovalent ions[33] but must be calculated from quantum chemical

https://dx.doi.org/10.1021/acs.jctc.0c00285
J. Chem. Theory Comput. 2020, 16, 5736−5746

simulations for the divalent carbonate ion. The ideal gas chemical potential is a function of the simulation density and can be written as

$$\mu^{\mathrm{IG}}_{M_2CO_3} = 3RT\ln\left(\frac{\sqrt[3]{4}N_{M_2CO_3}kT}{P_0\langle V\rangle_{M_2CO_3}}\right) \tag{10}$$

or

$$\mu^{\mathrm{IG}}_{\mathrm{MOH}} = 2RT\ln\left(\frac{N_{\mathrm{MOH}}kT}{P_0\langle V\rangle_{\mathrm{MOH}}}\right) \tag{11}$$

for carbonate and hydroxide, respectively. Here R is the gas constant, T is the temperature, N is the number of carbonate or hydroxide molecules, k is Boltzmann's constant, P_0 is the reference pressure at which $\Delta_f G^0$ is taken, and $\langle V\rangle$ is the equilibrium simulation volume. The expressions for the ideal gas chemical potentials of the neutral salt molecules are obtained by summing the chemical potentials of each ion in the molecule.

The excess chemical potential was calculated for the molten salts using Bennett's acceptance ratio (BAR).[34] For this calculation, the excess chemical potential is split into two pieces:

$$\mu^{\mathrm{EX}} = \mu^{\mathrm{EX}}_{\mathrm{vdW}} + \mu^{\mathrm{EX}}_{\mathrm{Coul}} \tag{12}$$

where $\mu^{\mathrm{EX}}_{\mathrm{vdW}}$ is the contribution from the Buckingham interactions and $\mu^{\mathrm{EX}}_{\mathrm{Coul}}$ is the contribution from the Coulomb interaction. A neutral salt molecule (M_2CO_3 or MOH) is inserted into the simulation in 37 steps over two stages corresponding to the two parts of μ^{EX} in eq 12. The interactions of the inserted molecule with the rest of the system are scaled as in eq 13.

$$U_{ij} = \lambda_A A_{ij}e^{-B_{ij}r_{ij}} - \lambda_C\frac{C_{ij}}{r_{ij}^6} + \lambda_q\frac{q_iq_j}{4\pi\epsilon_0 r_{ij}} \tag{13}$$

First, the non-Coulomb interactions are turned on by scaling the A parameter exponentially for 11 steps by λ_A, where

$$\lambda_A = \frac{e^{10\lambda} - 1}{e^{10} - 1} \tag{14}$$

and $\lambda = \{0, 0.1, ..., 0.9, 1\}$. The attractive part of the potential is then added in six steps by scaling C linearly with $\lambda_C = \{0, 0.2, ..., 0.8, 1\}$. The free energy change between each step is calculated using BAR, and the sum over all 16 steps gives $\mu^{\mathrm{EX}}_{\mathrm{vdW}}$. The Coulomb interactions are added in the second stage in 21 steps, scaling the charge by $\lambda_q = \{0, 0.11, 0.22, ..., 0.55, 0.6, 0.65, 0.7, 0.725, 0.75, ..., 1\}$. The free energy change from this insertion adds up to $\mu^{\mathrm{EX}}_{\mathrm{Coul}}$.

2.7. Formation Free Energy. Since there are no tabulated values for the free energy of formation of the carbonate ion, we employed quantum chemical simulations to compute $\Delta_f G^0$. All gas-phase quantum chemical calculations were performed using the Gaussian16 program.[28] To determine the most accurate method, we tested the predictions of several quantum chemical methods for the $\Delta_f G^0$ of water, carbon dioxide, and the hydroxide ion and validated against the available experimental data.[33] Based on our results, the G3MP2 method showed the best agreement with the reported thermochemical values and was used to calculate the $\Delta_f G^0$ of the carbonate ion. Details of these calculations and the validation can be obtained elsewhere.[13] The formation free energy of CO_3^{2-} obtained at the G3MP2 level is −130.12 kJ/mol at 923.15 K. All thermochemical values for the different species investigated here are provided in Table S2 of the Supporting Information.

2.8. Dynamic Properties. In order to validate the developed force fields, the ionic conductivity (σ) and viscosity (η) were calculated from the Green−Kubo expressions,[35−37] given in eqs 15 and 16, respectively.

$$\sigma = \frac{1}{3VkT}\int_0^\infty \mathbf{j}(0)\cdot\mathbf{j}(t)\mathrm{d}t \tag{15}$$

$$\eta = \frac{V}{10kT}\int_0^\infty \mathbf{P}(0):\mathbf{P}(t)\mathrm{d}t \tag{16}$$

In these equations, V represents the simulation volume, $\mathbf{j}$ is the electric current vector, and $\mathbf{P}$ is the pressure tensor.

To avoid any influence from a thermostat or barostat, the conductivity, viscosity, and diffusion coefficients were calculated in the *NVE* ensemble. First, the correct system volume for a pressure of 1 bar was determined from a 5 ns *NPT* simulation. Then, at the equilibrium volume, the system was equilibrated to the correct temperature in the *NVT* ensemble for 1 ns. Finally, the production runs were performed for 5 ns in the *NVE* ensemble. To ensure that energy was conserved, the *NVE* simulations were performed using GROMACS, v.2018, compiled with double precision. The uncertainty of these properties was determined by block averaging over five 1 ns blocks.

To capture the short-time behavior of the autocorrelation functions in eqs 15 and 16, the current and pressure tensor were output at every simulation step (1 fs). As can be seen in Figure S3 of the Supporting Information, the integral of the current autocorrelation function converged within 0.5 ps for the conductivity calculation. The autocorrelation function was calculated for 3 ps intervals, with starting points separated by 0.1 ps. The reported conductivities are the average value of the cumulative integral between 1 and 3 ps. For the viscosity, the integral in eq 16 converged in less than 15 ps for all of the salts, as seen in Figure S4 of the Supporting Information. The autocorrelation function was calculated for 30 ps intervals, with starting points separated by 0.1 ps. The reported viscosities are the average value of the cumulative integral between 20 and 30 ps.

Diffusion coefficients for each species were determined by a linear fit to the mean-squared displacement (MSD). The MSD was fit linearly between 100 and 900 ps for each 1 ns block. The fit was weighted based on the number of MSD points averaged for each time. Plots of the MSD for each species are given in Figures S5 and S6, showing that the system was in the diffusive regime over this time interval.

3. RESULTS AND DISCUSSION

3.1. AIMD Densities and RDFs. Table 1 shows the AIMD computed densities of unary and binary carbonates and for the unary hydroxides. As Table 1 demonstrates, AIMD-computed densities are in overall good agreement with the available experiments. The densities appear to be systematically underestimated, which could be due to inaccuracies in the approximate PBE-D3 functional. With the exception of refs 38 and 39, all reported measurements of molten MOH densities are within 3% of the AIMD computed values. We therefore conclude that AIMD can reasonably predict densities of molten alkali-metal carbonate and hydroxide salts. Due to the experimental scatter in the MOH densities, we used AIMD-

https://dx.doi.org/10.1021/acs.jctc.0c00285
J. Chem. Theory Comput. 2020, 16, 5736−5746

Table 1. Comparison of Experimental and AIMD Densities of Molten Carbonates and Hydroxides[a]

system	T (K)	exptl (kg m^{-3})	AIMD (kg m^{-3})
Li_2CO_3	1043.15	1813[40]	1794 (−1.0%)
Na_2CO_3	1173.15	1953[40]	1911 (−2.1%)
K_2CO_3	1213.15	1878[40]	1876 (−0.1%)
$Li_{0.6}K_{0.4}CO_3$	923.15	1938[40]	1877 (−3.1%)
$Li_{0.5}Na_{0.5}CO_3$	923.15	1961[40]	1920 (−2.5%)
LiOH	923.15	1362[41,b]	1387 (1.8%)
NaOH	923.15	1644[c]	1629 (−0.9%)
KOH	923.15	1642;[41] 1727[38]	1619 (−1.4%; −6.3%)

[a]Quantities in parentheses are the percent difference in AIMD values from experiment. [b]Extrapolated above experimental temperature range. [c]Average of five experimental values: 1655,[41] 1757,[38] 1635,[42] 1591,[43] and 1580.[39]

computed densities for parametrization of our M_2CO_3 and MOH force fields.

The good predictions of density provided by AIMD also give credence to the computed RDFs. The AIMD M−O and O−O RDFs, computed at the densities in Tables 1, are shown in Figure 3. The M−O RDFs show a clear first coordination shell for both carbonates and hydroxides. There is a clear trend in metal−oxygen distances increasing from Li to Na to K, as expected due to the increase in ionic radius going down the periodic table. Besides the intramolecular peak for carbonates, the O−O RDFs are much less structured, as would be expected from a mostly repulsive interaction.

3.2. GA Force Field Parametrization. Using the AIMD densities shown in Table 1, the AIMD RDFs shown in Figure 3, and the experimental enthalpy of formation from Table S1 of the Supporting Information, we performed two separate GA optimizations to generate the FFs, one for M_2CO_3 and one for MOH. Figure 4 shows the histogram of fitness values for the first 7 of the 10 GA generations for the MOH parameters. The optimization of the carbonate parameters showed very similar behavior.

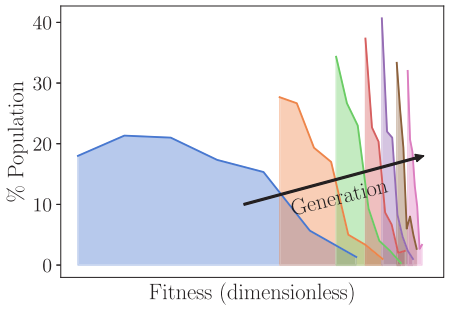

Figure 4. Histograms of population fitnesses with increasing number of generations, for GA optimization of MOH (M = Li, Na, K).

The initial population, which was created through the prescreening as detailed in Figure 1, shows a broad distribution of fitness values. Even one generation of GA significantly improved the fitness distribution. It is apparent that swapping traits between reasonably fit individuals is an efficient optimization strategy. This likely suggests that individual traits are not strongly coupled. For example, if one vector has superior M−O traits (e.g., RDF) and another vector has superior O−O traits, then it is often possible to create an offspring vector with M−O and O−O traits that are both superior, leading to higher total fitness than both parents. As can be seen in Figure 4, further generations both increase overall fitness and narrow the fitness diversity. After about 5−6 generations, further improvements are small. One possible reason for this is that at this point the fitness differences between individuals become approximately the same as the error in the density, RDF, and $\Delta_f H$ calculations due to a finite MD simulation time. A more detailed study of GA method efficiency would be highly informative but is beyond the scope of this work. For now, we conclude that GAs provide an attractive way to parametrize force fields for molten salts with large numbers of parameters.

All the nonbonded interaction potentials in molten carbonates and hydroxide parametrized in this work are

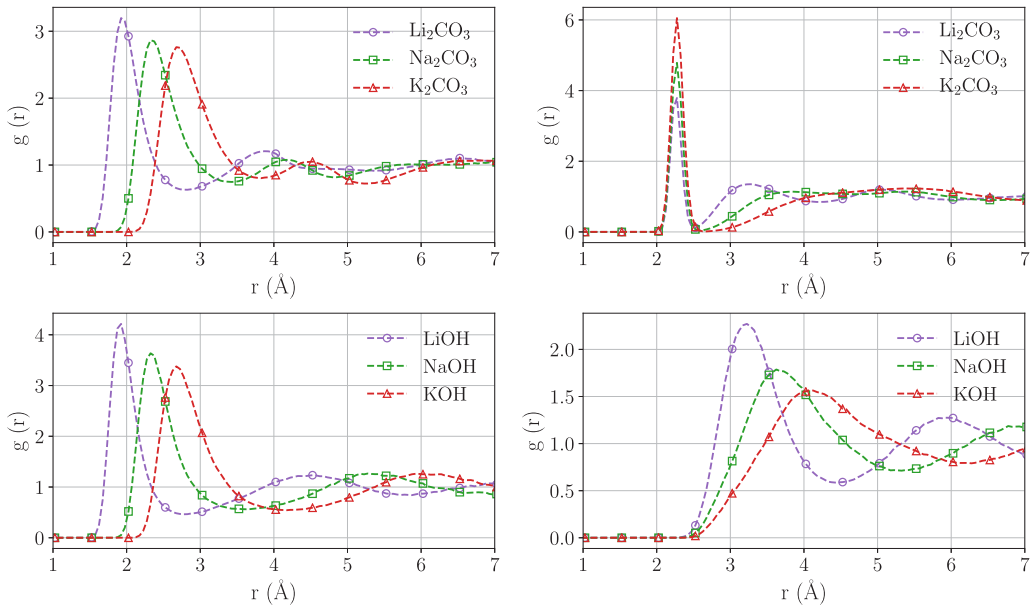

Figure 3. AIMD-computed radial distribution functions for molten alkali-metal carbonates (top panel) and hydroxides (bottom panel). Left: M−O; right: O−O RDFs.

https://dx.doi.org/10.1021/acs.jctc.0c00285
J. Chem. Theory Comput. 2020, 16, 5736−5746

tabulated in Tables 2 and 3. The bonded force field parameters parametrized in this study are summarized in Table 4.

Table 2. Atomic Site Charges (q) for Different Atom Types in the Alkali Carbonate and Hydroxide Molecules Parameterized in This Work

atom type	charge, q(e)
C_1 (C in CO_3^{2-})	1.44640
O_1 (O in CO_3^{2-})	−1.14880
H_1 (H in OH^-)	0.27696
O_2 (O in OH^-)	−1.27696
Li	1.0
Na	1.0
K	1.0

Table 3. Nonbonded Force Field Parameters A_{ij} and B_{ij} for the Repulsive and C_{ij} for the Dispersive Terms of the Interaction Potential in Eq 2[a]

pair	A_{ij} (kJ/mol)	B_{ij} (nm^{-1})	C_{ij} (kJ nm^6/mol)
O_1–O_1	2.69×10^6	46.35	1.90×10^{-3}
O_1–Li	1.24×10^5	40.65	3.10×10^{-5}
O_1–Na	2.57×10^5	39.23	3.42×10^{-4}
O_1–K	1.74×10^5	32.63	3.80×10^{-3}
O_2–O_2	2.87×10^6	52.61	9.61×10^{-4}
O_2–Li	4.91×10^4	34.48	2.61×10^{-4}
O_2–Na	9.42×10^4	31.86	3.18×10^{-3}
O_2–K	1.37×10^5	30.15	6.32×10^{-3}
O_2–H_1	3.02×10^6	60.41	6.08×10^{-4}

[a]All Buckingham pair parameters not shown are set to zero.

Table 4. Harmonic Potentials for the Bonded Terms in Carbonate and Hydroxide Ions[a]

bond	r_{eq} (nm)	k_{eq} (kJ/mol)
C_1–O_1	0.130	6.12×10^5
O_2–H_1	0.098	—
angle	θ_{eq} (deg)	k_{eq} (kJ/mol/rad^2)
O_1–C_1–O_1	120.0	1.19×10^3
dihedral	θ_{eq} (deg)	k_{eq} (kJ/mol)
O_1–C_1–O_1–O_1	180.0	2.68×10^2

[a]k_{eq} is not specified for the rigid bonds.

3.3. GA Force Field Predictions. Figure 5 compares the temperature dependence of the density of the GA force field with one set of experiments and AIMD. For all of the salts, the GA force field agrees with AIMD to within 20 kg/m^3. However, the experimental results for some salts, especially LiOH and Na_2CO_3, differ by ∼2% from the results of the GA force field and AIMD. However, these differences are comparable in magnitude to the scatter in experimental values seen for the other salts.[38−44]

The CR and JT carbonate models are also plotted for comparison. The CR model performs similarly to the GA force field, but the JT model predicts a density 10−20% below that of the other force fields. The thermal expansion coefficient is predicted well by all carbonate force fields, but it is overestimated by the GA force field for KOH and underestimated for LiOH.

The chemical potential of the molten salts is a key property for the force field since it is necessary for the calculation of thermodynamic properties such as reaction equilibria. The

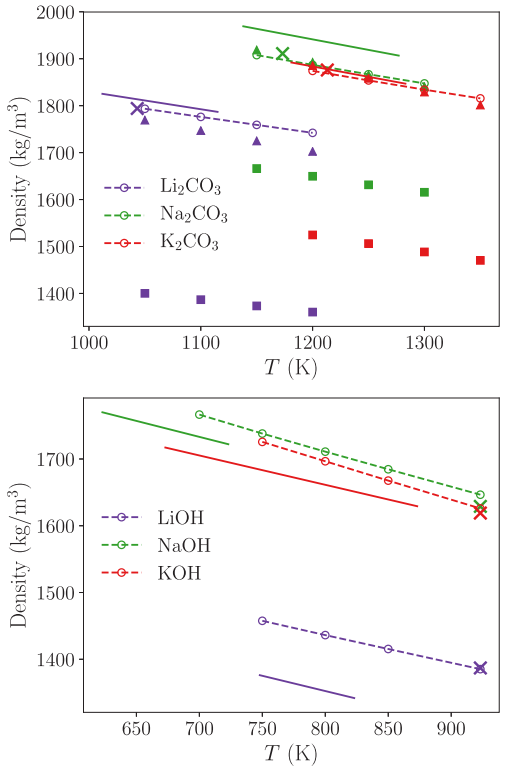

Figure 5. Density of molten salts obtained from simulations employing the optimized force field (GA) parameters and compared against *ab initio* molecular dynamics (AIMD), existing carbonate force fields, and experimental data. Empty circles and dashed line, GA force field; crosses, AIMD; triangles, Corradini et al.;[16,17] squares, Janssen-Tissen;[14] and solid lines, experiment.[40] Top panel: molten carbonates; bottom panel: molten hydroxides.

chemical potential of the GA model is compared with experimental values from the NIST-JANAF thermochemical tables in Figure 6. The GA force field performs well for all of the salts, with a maximum deviation of ∼12 kJ/mol for K_2CO_3, indicating that fitting the density, RDF, and enthalpy of formation is sufficient to ensure accurate chemical potentials. This is an important observation, suggesting that the (expensive) chemical potential calculations need not be performed repeatedly during parameter optimization. The JT model[14] is slightly worse than the GA results, while the CR[16,17] force field gives considerably more positive chemical potentials than the experiments, with typical deviations of more than 200 kJ/mol. Since the CR model uses scaled charges, the magnitude of the free energy change from inserting a molecule will be smaller since less charge is inserted into the system. Therefore, the chemical potential will be overpredicted. This observation motivated our choice of full charges for the ions in the GA force field. While using scaled-charge models is a common method to correct for lack of polarizability in classical electrolyte force fields,[45] their use is detrimental to other properties, for example, the modeling of chemical reaction equilibria among charged species in condensed phases.

Tables 5 and 6 give the viscosity and the ionic conductivity, respectively, of the unary salts and mixed carbonates. The viscosity of the GA models is always higher than that of experiments. Conversely, the ionic conductivity of the GA force field is always lower than that of experiments. Both of these deviations indicate that the dynamics in the simulation are slower than they should be. It has been observed previously

https://dx.doi.org/10.1021/acs.jctc.0c00285
J. Chem. Theory Comput. 2020, 16, 5736−5746

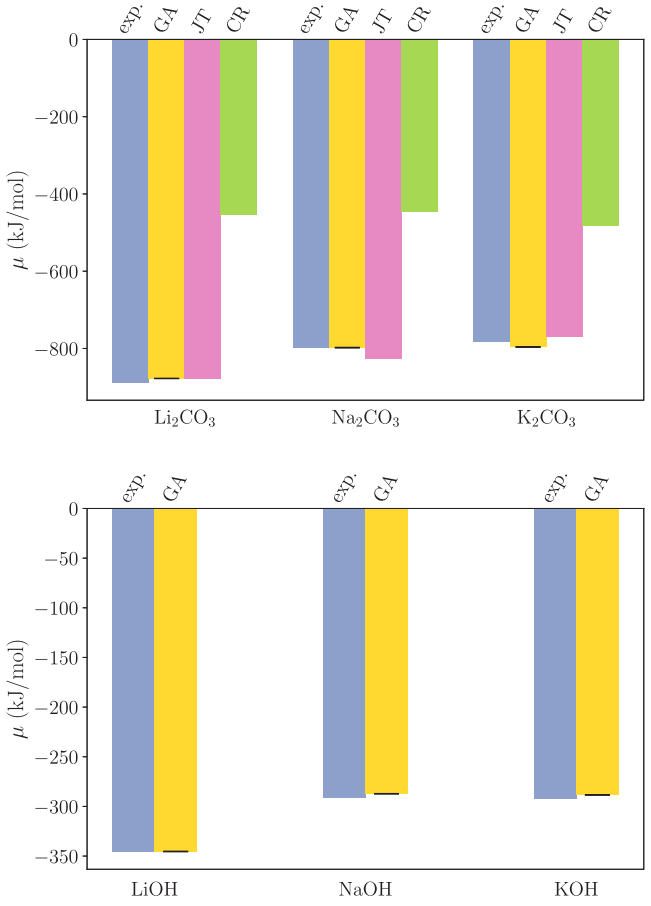

Figure 6. Chemical potential of molten salts obtained from simulations employing the optimized force field (GA) parameters and compared against experimental data.[33] Top panel: molten carbonates at 1200 K compared with other existing carbonate models, JT,[14] and CR.[16,17] Bottom panel: molten hydroxides at 923.15 K. Uncertainties for the GA force field represent one standard error.

Table 5. Viscosity, η (cP), and Percent Deviation, $\Delta\eta$ ($\Delta\eta = 100(\eta_{sim} - \eta_{exp})/\eta_{exp}$), from Experiment[40] of Molten Salts and Eutectic Compositions Obtained from Simulations Employing the Optimized Force Field (GA) Parameters[a]

system	T (K)	η_{exp}	η_{sim}	$\Delta\eta$ (%)
Li_2CO_3	1101	4.9	7.3 ± 0.7	50
Na_2CO_3	1198	3.4	4.3 ± 0.1	25
K_2CO_3	1180	3.0	4.1 ± 0.2	37
$Li_{0.4}K_{0.6}CO_3$	1100	3.3	6.2 ± 0.4	89
$Li_{0.6}K_{0.4}CO_3$	1103	3.5	7.1 ± 0.2	103
$Li_{0.5}Na_{0.5}CO_3$	1106	4.1	6.4 ± 0.4	57
$Na_{0.5}K_{0.5}CO_3$	1105	3.9	5.3 ± 0.3	36
LiOH	805	—	2.2 ± 0.1	—
NaOH	710	2.4	3.6 ± 0.1	52
KOH	839	0.9	1.7 ± 0.1	78

[a]Uncertainties represent one standard error.

for both ionic liquids[45] and electrolyte solutions[46] that dynamics of full-charge models tend to be too slow relative to scaled charge models. This is illustrated by the CR model which shows a better prediction of viscosity (3.04 cP) and ionic conductivity (228.4 S/m) than the GA force field for $Li_{0.62}K_{0.38}CO_3$ at 1100 K.[16] However, since the deviations from experiments are consistent across the different salts for the GA force field, conclusions on relative trends still hold true for dynamic properties. The quantitative values for the GA force field are an average of 30% lower for conductivity (with a standard deviation of 12%) and 58% higher for viscosity (with a standard deviation of 30%).

Table 6. Ionic Conductivity, σ (S/m), and Percent Deviation, $\Delta\sigma$ ($\Delta\sigma = 100(\sigma_{sim} - \sigma_{exp})/\sigma_{exp}$), from Experiment[40] of Molten Salts and Eutectic Compositions Obtained from Simulations Employing the Optimized Force Field (GA) Parameters[a]

system	T (K)	σ_{exp}	σ_{sim}	$\Delta\sigma$ (%)
Li_2CO_3	1101	482	269 ± 22	−44
Na_2CO_3	1198	313	223 ± 9	−29
K_2CO_3	1180	205	174 ± 6	−15
$Li_{0.4}K_{0.6}CO_3$	1100	201	139 ± 5	−31
$Li_{0.6}K_{0.4}CO_3$	1103	240	134 ± 12	−44
$Li_{0.5}Na_{0.5}CO_3$	1106	325	187 ± 10	−43
$Na_{0.5}K_{0.5}CO_3$	1105	207	145 ± 5	−30
LiOH	805	—	627 ± 35	—
NaOH	710	316	288 ± 5	−9
KOH	839	348	252 ± 3	−28

[a]Uncertainties represent one standard error.

The diffusion coefficient of each ion is given in Tables S3 and S4 of the Supporting Information. Experimental results could only be found for Na_2CO_3. At a temperature of 1197.9 K, the experimental diffusion of the Na^+ ion is 6.02×10^{-5} cm^2/s and that of the CO_3^{2-} ion is 3.30×10^{-5} cm^2/s.[47] The GA force field predicts diffusion coefficients of 3.74×10^{-5} and 1.24×10^{-5} cm^2/s for these ions, respectively. The experimental values are both higher than the simulations, indicating that again the dynamics are slow for full-charge models.

The ultimate aim for the force fields parametrized here is to compute the reaction equilibrium and transport properties of hydroxide−carbonate mixtures.Therefore, to test the applicability of these force fields to mixtures, we compared the densities of sodium carbonate−hydroxide and potassium carbonate−hydroxide mixtures as a function of hydroxide concentration against experimental measurements in Figure 7. We used Mason−Rice combining rules[48,49] for the hydroxide−carbonate cross-interactions (arithmetic mean for the size and geometric mean for the energy parameters). These combining

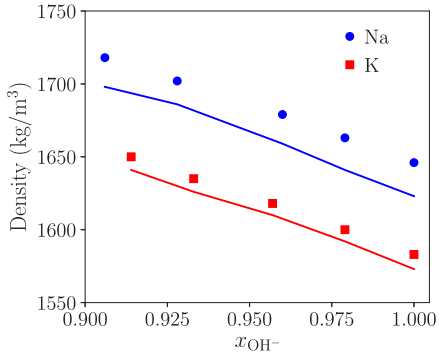

Figure 7. Density of sodium carbonate−hydroxide and potassium carbonate−hydroxide mixtures as a function of hydroxide ion concentration. The solid lines represent experiments while symbols show simulated values. The simulation uncertainties are smaller than the data points.

https://dx.doi.org/10.1021/acs.jctc.0c00285
J. Chem. Theory Comput. 2020, 16, 5736−5746

rules are sufficient since the interactions between the negatively charged carbonate and hydroxide ions are expected to be dominated by Coulomb repulsion. Based on the available experimental data, the simulation temperature for the sodium and potassium salt mixtures was set to 923.15 and 1000.0 K, respectively. The system size used for these simulations was as close to 1000 cations as possible to reach the concentrations at which experimental data were available.

Figure 7 reveals a very good agreement between the computed density and the experimental values, with a maximum deviation of ∼1.4%. The deviation remains approximately constant as the composition changes, justifying our choice of cross-interaction parameters between carbonate and hydroxide ions. The difference in densities of the pure hydroxide systems is expected because the force field was fit against the *ab initio* density instead of experimental data. Therefore, the force fields presented in this work can also be used to model mixed carbonate−hydroxide systems.

4. CONCLUSIONS

Since the existing JT[14] and CR[16,17] models were found to be inadequate in simultaneously predicting chemical potential and density for carbonates, and since there are no force fields available to describe mixed carbonate−hydroxide melts, in this work we parametrized a new classical force field for molten alkali-metal carbonate and hydroxide salts. Our force field is able to accurately predict both liquid phase chemical potential and density because of the rigorous optimization process utilized during force field development. Unlike previous models, it is capable of describing chemical potentials of the charged species in condensed phases.

We employed AIMD computed densities, RDFs, and experimental enthalpy of formation to optimize the force field parameters. The AIMD computed densities are in agreement with experiments, implying that PBE-D3 is a reliable choice for molten salts. In order to obtain the correct chemical potential for the salts, we included the liquid enthalpy of formation as a fitting property since enthalpy is an important component in chemical potential. We chose a genetic algorithm for the optimization because the force fields involve a large set of parameters. The genetic algorithm was able to reliably reproduce the fit properties within 5−6 generations. This illustrates the efficiency of genetic algorithms over manual tuning of parameters.

We found that full charges on ions are required to obtain chemical potentials for molten phases comparable to experiments. This motivated our selection of full charges for the carbonate and hydroxide ions. The disadvantage of this choice is that a full charge force field has slower dynamics than experiments. The GA force field underestimates the ionic conductivity by an average of 30% and overestimates viscosity by 58% on average. However, the deviation in transport properties is consistent across different systems, allowing for predictions of relative trends in these properties. Polarizability is likely required for a force field to correctly predict both chemical potential and dynamics for molten salts, as seems to be also the case for electrolyte solutions.[46]

The accuracy of this force field for pure chemical potentials as well as for the carbonate−hydroxide mixture density suggests that these parameters are applicable for investigating the carbonate−hydroxide mixture reaction equilibrium in eq 1, as we report in a separate paper.[13] The accurate mixture behavior will also allow for future study of trends in transport properties for carbonate−hydroxide mixtures. The protocol presented here illustrates a reliable path for obtaining force field parameters for ionic systems with accurate thermodynamic properties.

■ ASSOCIATED CONTENT

Supporting Information

The Supporting Information is available free of charge at https://pubs.acs.org/doi/10.1021/acs.jctc.0c00285.

Table of the enthalpy of formation of molten salts, potential energy surfaces in carbonate ion, table of the formation free energy of each species, running integrals of ionic conductivity and shear viscosity, mean-square displacements of ions, and tables of diffusion coefficients of ions in molten salts (PDF)

■ AUTHOR INFORMATION

Corresponding Authors

Lucas Koziol − *ExxonMobil Research and Engineering, Annandale, New Jersey 08801, United States*; Email: lucas.koziol@exxonmobil.com

Athanassios Z. Panagiotopoulos − *Department of Chemical and Biological Engineering, Princeton University, Princeton, New Jersey 08544, United States*; orcid.org/0000-0002-8152-6615; Email: azp@princeton.edu

Authors

Anirban Mondal − *Department of Chemical and Biological Engineering, Princeton University, Princeton, New Jersey 08544, United States*; orcid.org/0000-0003-3029-8840

Jeffrey M. Young − *Department of Chemical and Biological Engineering, Princeton University, Princeton, New Jersey 08544, United States*; orcid.org/0000-0001-8879-5132

Timothy A. Barckholtz − *ExxonMobil Research and Engineering, Annandale, New Jersey 08801, United States*

Gabor Kiss − *ExxonMobil Research and Engineering, Annandale, New Jersey 08801, United States*

Complete contact information is available at: https://pubs.acs.org/10.1021/acs.jctc.0c00285

Notes

The authors declare the following competing financial interest(s): The Princeton authors declare no potential conflict of interest. T.A.B., G.K., and L.K. are all employees of ExxonMobil, which is currently working on commercializing MCFCs in the industrial and power sectors.

■ ACKNOWLEDGMENTS

Financial support for this work was provided by ExxonMobil, under agreement EM09125.A1, and by the Office of Basic Energy Sciences, U.S. Department of Energy, under Award DE-SC0002128. Computing resources were provided by Princeton Research Computing.

■ REFERENCES

(1) Gaillard, F.; Malki, M.; Iacono-Marziano, G.; Pichavant, M.; Scaillet, B. Carbonatite Melts and Electrical Conductivity in the Asthenosphere. *Science* **2008**, *322*, 1363−1365.

(2) Jones, A. P.; Genge, M.; Carmody, L. Carbonate Melts and Carbonatites. *Rev. Mineral. Geochem.* **2013**, *75*, 289−322.

(3) Chery, D.; Lair, V.; Cassir, M. CO_2 Electrochemical Reduction into CO or C in Molten Carbonates: A Thermodynamic Point of View. *Electrochim. Acta* **2015**, *160*, 74−81.

(4) Cassir, M.; McPhail, S. J.; Moreno, A. Strategies and New Developments in the Field of Molten Carbonates and High-Temperature Fuel Cells in the Carbon Cycle. *Int. J. Hydrogen Energy* **2012**, *37*, 19345−19350.
(5) Dasgupta, R.; Hirschmann, M. M. The Deep Carbon Cycle and Melting in Earth's Interior. *Earth Planet. Sci. Lett.* **2010**, *298*, 1−13.
(6) Tomczyk, P. MCFC Versus Other Fuel Cells-Characteristics, Technologies and Prospects. *J. Power Sources* **2006**, *160*, 858−862.
(7) Caprile, L.; Passalacqua, B.; Torazza, A. Carbon Capture: Energy Wasting Technologies or the MCFCs Challenge? *Int. J. Hydrogen Energy* **2011**, *36*, 10269−10277.
(8) Wee, J. H. Carbon Dioxide Emission Reduction Using Molten Carbonate Fuel Cell Systems. *Renewable Sustainable Energy Rev.* **2014**, *32*, 178−191.
(9) Sangarunlert, W.; Suhchai, S.; Nathakaranakule, A. Molten Carbonate Fuel Cell (MCFC) Characteristics, Technologies and Economic Analysis: Review. *Int. J. Renew. Energy* **2008**, *3*, 1−9.
(10) Rao, A. B.; Rubin, E. S. A Technical, Economic, and Environmental Assessment of Amine-Based CO_2 Capture Technology for Power Plant Greenhouse Gas Control. *Environ. Sci. Technol.* **2002**, *36*, 4467−4475.
(11) Manzolini, G.; Campanari, S.; Chiesa, P.; Giannotti, A.; Bedont, P.; Parodi, F. CO_2 Separation from Combined Cycles Using Molten Carbonate Fuel Cells. *J. Fuel Cell Sci. Technol.* **2012**, *9*, 011018.
(12) Rosen, J.; Geary, T.; Hilmi, A.; Blanco-Gutierrez, R.; Yuh, C.-Y.; Pereira, C. S.; Han, L.; Johnson, R. A.; Willman, C. A.; Ghezel-Ayagh, H.; Barckholtz, T. A. Performance of Molten Carbonate Fuel Cells for Deep CO_2 Capture from Natural Gas Combined Cycle Flue Gas. *J. Electrochem. Soc.* **2020**, *167*, 064505.
(13) Young, J. M.; Mondal, A.; Barckholtz, T. A.; Kiss, G.; Koziol, L.; Panagiotopoulos, A. Z. Predicting Chemical Reaction Equilibria in Molten Carbonate Fuel Cells via Molecular Simulations. *AIChE J.* **2020**, DOI: 10.1002/aic.16988.
(14) Tissen, J. T.; Janssen, G. J. Molecular-Dynamics Simulation of Molten Alkali Carbonates. *Mol. Phys.* **1990**, *71*, 413−426.
(15) Costa, M. F. Molecular Dynamics of Molten Li_2CO_3-K_2CO_3. *J. Mol. Liq.* **2008**, *138*, 61−68.
(16) Corradini, D.; Coudert, F. X.; Vuilleumier, R. Insight Into the Li_2CO_3-K_2CO_3 Eutectic Mixture from Classical Molecular Dynamics: Thermodynamics, Structure, and Dynamics. *J. Chem. Phys.* **2016**, *144*, 104507.
(17) Desmaele, E.; Sator, N.; Vuilleumier, R.; Guillot, B. Atomistic Simulations of Molten Carbonates: Thermodynamic and Transport Properties of the Li_2CO_3-Na_2CO_3-K_2CO_3 System. *J. Chem. Phys.* **2019**, *150*, 094504.
(18) Okazaki, S.; Ohtori, N.; Okada, I. Molecular Dynamics Studies on Molten Alkali Hydroxides. I. Static Properties of Molten LiOH. *J. Chem. Phys.* **1990**, *92*, 7505−7514.
(19) Perdew, J. P.; Burke, K.; Ernzerhof, M. Generalized Gradient Approximation Made Simple. *Phys. Rev. Lett.* **1996**, *77*, 3865−3868.
(20) Grimme, S.; Antony, J.; Ehrlich, S.; Krieg, H. A Consistent and Accurate *Ab Initio* Parametrization of Density Functional Dispersion Correction (DFT-D) for the 94 Elements H-Pu. *J. Chem. Phys.* **2010**, *132*, 154104.
(21) Hutter, J.; Iannuzzi, M.; Schiffmann, F.; VandeVondele, J. CP2K: Atomistic Simulations of Condensed Matter Systems. *Wiley Interdiscip. Rev.: Comput. Mol. Sci.* **2014**, *4*, 15−25.
(22) Goedecker, S.; Teter, M.; Hutter, J. Separable Dual-Space Gaussian Pseudopotentials. *Phys. Rev. B: Condens. Matter Mater. Phys.* **1996**, *54*, 1703−1710.
(23) Hartwigsen, C.; Goedecker, S.; Hutter, J. Relativistic Separable Dual-Space Gaussian Pseudopotentials from H to Rn. *Phys. Rev. B: Condens. Matter Mater. Phys.* **1998**, *58*, 3641−3662.
(24) Martyna, G. J.; Tobias, D. J.; Klein, M. L. Constant Pressure Molecular Dynamics Algorithms. *J. Chem. Phys.* **1994**, *101*, 4177−4189.
(25) Martyna, G. J.; Klein, M. L.; Tuckerman, M. Nosé-Hoover Chains: The Canonical Ensemble via Continuous Dynamics. *J. Chem. Phys.* **1992**, *97*, 2635−2643.
(26) Bengtson, A.; Nam, H. O.; Saha, S.; Sakidja, R.; Morgan, D. First-Principles Molecular Dynamics Modeling of the LiCl-KCl Molten Salt System. *Comput. Mater. Sci.* **2014**, *83*, 362−370.
(27) Li, Y.; Li, H.; Pickard, F. C.; Narayanan, B.; Sen, F. G.; Chan, M. K. Y.; Sankaranarayanan, S. K. R. S.; Brooks, B. R.; Roux, B. Machine Learning Force Field Parameters from *Ab Initio* Data. *J. Chem. Theory Comput.* **2017**, *13*, 4492−4503.
(28) Frisch, M. J.; Trucks, G. W.; Schlegel, H. B.; Scuseria, G. E.; Robb, M. A.; Cheeseman, J. R.; Scalmani, G.; Barone, V.; Petersson, G. A.; Nakatsuji, H.; Li, X.; Caricato, M.; Marenich, A. V.; Bloino, J.; Janesko, B. G.; Gomperts, R.; Mennucci, B.; Hratchian, H. P.; Ortiz, J. V.; Izmaylov, A. F.; Sonnenberg, J. L.; Williams-Young, D.; Ding, F.; Lipparini, F.; Egidi, F.; Goings, J.; Peng, B.; Petrone, A.; Henderson, T.; Ranasinghe, D.; Zakrzewski, V. G.; Gao, J.; Rega, N.; Zheng, G.; Liang, W.; Hada, M.; Ehara, M.; Toyota, K.; Fukuda, R.; Hasegawa, J.; Ishida, M.; Nakajima, T.; Honda, Y.; Kitao, O.; Nakai, H.; Vreven, T.; Throssell, K.; Montgomery, J. A., Jr.; Peralta, J. E.; Ogliaro, F.; Bearpark, M. J.; Heyd, J. J.; Brothers, E. N.; Kudin, K. N.; Staroverov, V. N.; Keith, T. A.; Kobayashi, R.; Normand, J.; Raghavachari, K.; Rendell, A. P.; Burant, J. C.; Iyengar, S. S.; Tomasi, J.; Cossi, M.; Millam, J. M.; Klene, M.; Adamo, C.; Cammi, R.; Ochterski, J. W.; Martin, R. L.; Morokuma, K.; Farkas, O.; Foresman, J. B.; Fox, D. J. *Gaussian16*, Revision C.01; Gaussain, Inc.: Wallingford, CT, 2016.
(29) Hess, B.; Kutzner, C.; Van Der Spoel, D.; Lindahl, E. GROMACS 4: Algorithms for Highly Efficient, Load-Balanced, and Scalable Molecular Simulation. *J. Chem. Theory Comput.* **2008**, *4*, 435−447.
(30) Pronk, S.; Páll, S.; Schulz, R.; Larsson, P.; Bjelkmar, P.; Apostolov, R.; Shirts, M. R.; Smith, J. C.; Kasson, P. M.; van der Spoel, D.; Hess, B.; Lindahl, E. GROMACS 4.5: A High-Throughput and Highly Parallel Open Source Molecular Simulation Toolkit. *Bioinformatics* **2013**, *29*, 845−854.
(31) Bussi, G.; Donadio, D.; Parrinello, M. Canonical Sampling Through Velocity Rescaling. *J. Chem. Phys.* **2007**, *126*, 014101.
(32) Parrinello, M.; Rahman, A. Polymorphic Transitions in Single Crystals: A New Molecular Dynamics Method. *J. Appl. Phys.* **1981**, *52*, 7182−7190.
(33) Chase, M. W. *NIST-JANAF Thermochemical Tables*, 4th ed.; American Chemical Society: Washington, DC, 1998.
(34) Bennett, C. H. Efficient Estimation of Free Energy Differences from Monte Carlo Data. *J. Comput. Phys.* **1976**, *22*, 245−268.
(35) Harada, M.; Yamanaka, A.; Tanigaki, M.; Tada, Y. Mass and Size Effects on the Transport Properties of Molten Salts. *J. Chem. Phys.* **1982**, *76*, 1550−1556.
(36) Daivis, P. J.; Evans, D. J. Comparison of Constant Pressure and Constant Volume Nonequilibrium Simulations of Sheared Model Decane. *J. Chem. Phys.* **1994**, *100*, 541−547.
(37) Hansen, J.-P.; McDonald, I. R. *Theory of Simple Liquids: with Applications to Soft Matter*, 4th ed.; Academic Press: New York, 2013.
(38) Janz, G. J.; Dampier, F. W.; Lakshminarayan, G. R.; Lorenz, P. K.; Tomkins, R. P. T. *Molten Salts. Vol. 1. Electrical Conductance, Density, and Viscosity Data*; National Bureau of Standards: New York, 1968.
(39) Arndt, K.; Ploetz, G. Conductivity and Viscosity of Molten NaOH and KOH. *Z. Phys. Chem.* **1926**, *121*, 439−455.
(40) Janz, G. J. Thermodynamic and Transport Properties for Molten Salts: Correlation Equations for Critically Evaluated Density, Surface Tension, Electrical Conductance, and Viscosity Data. *J. Phys. Chem. Ref. Data* **1988**, *17*, Suppl. 2.
(41) Claes, P.; Gilbert, J. Electrical Conductivity and Specific Mass of the Molten LiOH-$LiNO_3$, NaOH-$NaNO_3$, and KOH-KNO_3, Mixtures. *J. Electrochem. Soc.* **1985**, *132*, 857−862.
(42) Bogart, D. Densities of Molten Sodium and Rubidium Hydroxides. *J. Phys. Chem.* **1954**, *58*, 1168−1169.
(43) Patrov, B. V.; Yurkinskii, V. P. Surface Tension and Density of a Sodium Hydroxide Melt. *Russ. J. Appl. Chem.* **2004**, *77*, 2029−2030.
(44) Kojima, T.; Miyazaki, Y.; Nomura, K.; Tanimoto, K. Physical Properties of Molten Li_2CO_3-Na_2CO_3 (52:48 mol%) and Li_2CO_3-

K_2CO_3 (62:38 mol%) Containing Additives. *J. Electroanal. Chem.* **2013**, *160*, 733−741.
(45) Youngs, T. G.; Hardacre, C. Application of Static Charge Transfer Within an Ionic-Liquid Force Field and its Effect on Structure and Dynamics. *ChemPhysChem* **2008**, *9*, 1548−1558.
(46) Yue, S.; Panagiotopoulos, A. Z. Dynamic Properties of Aqueous Electrolyte Solutions from Non-Polarisable, Polarisable, and Scaled-Charge Models. *Mol. Phys.* **2019**, *117*, 3538−3549.
(47) Janz, G. J.; Bansal, N. P. Molten Salts Data: Diffusion Coefficients in Single and Multi Component Salt Systems. *J. Phys. Chem. Ref. Data* **1982**, *11*, 505−693.
(48) Mason, E. A.; Rice, W. E. The Intermolecular Potentials of Helium and Hydrogen. *J. Chem. Phys.* **1954**, *22*, 522−535.
(49) Mirskaya, K. V. Combining Rules for Interatomic Potential Functions of Buckingham Form. *Tetrahedron* **1973**, *29*, 679−682.

https://dx.doi.org/10.1021/acs.jctc.0c00285
J. Chem. Theory Comput. 2020, 16, 5736−5746